ACS Macro Letters

Letter

pubs.acs.org/macroletters

Nonisotropic Self-Organization of Single-Component Hairy Nanoparticle Assemblies

Hilmar Koerner,[†] Lawrence F. Drummy,[†] Brian Benicewicz,[§] Yu Li,[‡] and Richard A. Vaia*[,†]

[†]Air Force Research Laboratory, WPAFB, Dayton, Ohio 45433, United States

[‡]Department of Chemistry, Rensselaer Polytechnic Institute, Troy, New York 12180, United States

[§]Department of Chemistry and Biochemistry, University of South Carolina, Columbia, South Carolina 29201, United States

Supporting Information

ABSTRACT: Solvent-free assemblies of hairy nanoparticles (HNPs) are providing avenues to avoid issues of mixing, agglomeration, and limited inorganic content that plague nanocompositses based on polymer−nanoparticle blending. Here we demonstrate that the order within, and the elongational characteristics of, the neat HNP assembly (aHNP) evolve as the architecture of the polymeric corona in solution transitions from the concentrated (CPB) to semidilute (SDPB) polymer brush regimes (silica nanoparticle: radius r_0 = 8 nm with 120 kDa polystyrene grafts at σ = 0.01−0.1 chains/nm^2). Specifically, local HNP packing adopts a nonisotropic local arrangement at intermediate graft densities where the transition from CPB-to-SDPB in solution is approximately r_0. In concert, the neat HNP assembly responds to viscoelastic elongational deformation in a manner analogous to semicrystalline elastomers. Domain orientation under load and subsequent buckling upon recovery lead to the appearance of two- and four-point small-angle X-ray patterns. The correlation between the corona architecture of the HNP and the physical characteristics of the solvent-free aHNP provides a framework akin to block-copolymers to tune mechanical, optical, and electrical properties of fibers and films via ordered mesoscale morphology.

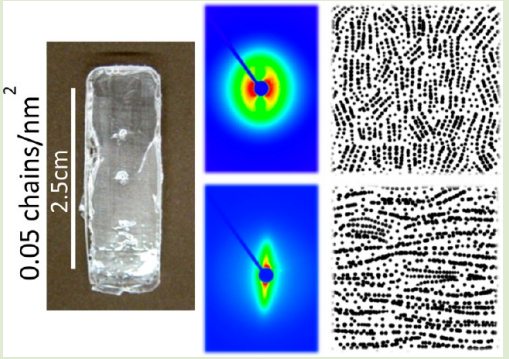

Polymer nanocomposites (PNCs) are a blend of inorganic nanoparticles (NPs) and polymer, where the nanoscale morphology, increased number density of filler, and propensity of internal interfaces in some instances leads to enhanced thermal, mechanical, and electrical performance relative to micro- and macroscale filled polymer counterparts.[1] As such, they are of significant interest for a wide array of structural and multifunctional applications including lightweight transportation, high performance aerospace components, and food and beverage packaging.[2] The enhancements depend strongly on the NP dispersion and the nature (strength and toughness) of the NP−polymer interface.[1,3,4] Fundamentally, these key factors are coupled and depend on the chemistry, molecular interactions, width, and penetrability of the initial NP−NP interface in the aggregate and final NP−matrix interfaces in the dispersion. The use of polymer brushes, in lieu of small molecular compatibilizers, has recently shown substantial promise in affording additional tunability and modularity to optimize these factors for a given NP−polymer combination.[5−8] In general, these "hairy" nanoparticles (HNPs) consist of a nanoparticle core surrounded by end-grafted polymer chains ranging from low to high molecular weight.[9]

Recently, solvent-free assemblies (aHNPs) of these "hairy" nanoparticles have garnered substantial technological interest due to their inherent ability to avoid aggregation issues that limit scalability and reliability of traditional PNCs for many functional (optical, dielectric, and magnetic) applications.[10−13] By grafting the polymer to the nanoparticle, the desired composition and morphology are an intrinsic characteristic of the macroscopic material. However, a complete understanding of the relationship between the characteristics of the HNP and the structure, processability, and properties of the assembly is still in its infancy. To the first order, the corona structure of spherical HNPs in solution can be described by an extension of the polymer brush model of Alexander and de Gennes,[14,15] such as that developed by Daoud and Cotton for star polymers.[16] The key geometrical constraint underlying these descriptions is that the volume per chain increases radially from the inorganic core and thus results in a concomitant change in the chain conformation. Recent experimental work by Dukes et al. suggests that the model developed by Wijmans and Zhulina (WZ)[17] is the most versatile in describing the conformation of the brush in solution at intermediate to high graft densities.[18] Overall, the characteristics of this polymer corona can be understood based on the nanoparticle curvature (r_o^{-1}), graft density (σ), and chain molecular weight (N). In a good solvent, three regimes can be discussed, where mushroom ($\sigma < 1/R_g^2$) and concentrated polymer brush (CPB) regimes bracket semidilute polymer brush (SDPB) architectures. Note that R_g is the radius of gyration of the chain, where $R_g \sim \Lambda N^{-1/2}$ and Λ

Received: April 11, 2013
Accepted: July 1, 2013

 © XXXX American Chemical Society dx.doi.org/10.1021/mz4001805 | ACS Macro Lett. 2013, 2, 670−676

Table 1. Morphology of HNPs and aHNPs[a]

	wt/vol fraction SiO_2 (TGA)	σ chains/nm^2	# of chains/NP	L_{TGA}/nm	L_{SAX}/nm	r_c/nm	T_g/°C
SiPS0p01	0.65/0.47	0.01	8	19.1	18	5.1	80
SiPS0p05	0.32/0.18	0.05	40	26.5	42	11.4	75
SiPS0p1	0.18/0.09	0.1	80	32.1	31	16.1	75

[a] $r_c = r_0\sigma_0^{*1/2}\nu^{*-1}$, [9] $\sigma^* = \sigma l_0^2$ (l_0 = 0.9 nm), $\nu^* = (4\pi)^{1/2}\nu$ (ν = 0.5 for theta solvent). r_0 = 8 nm; ν is the excluded volume parameter; ν^* is the reduced excluded volume parameter; σ is graft density; σ^* is reduced graft density; r_c is the radius of transition from the CPB-to-SDPB regime.

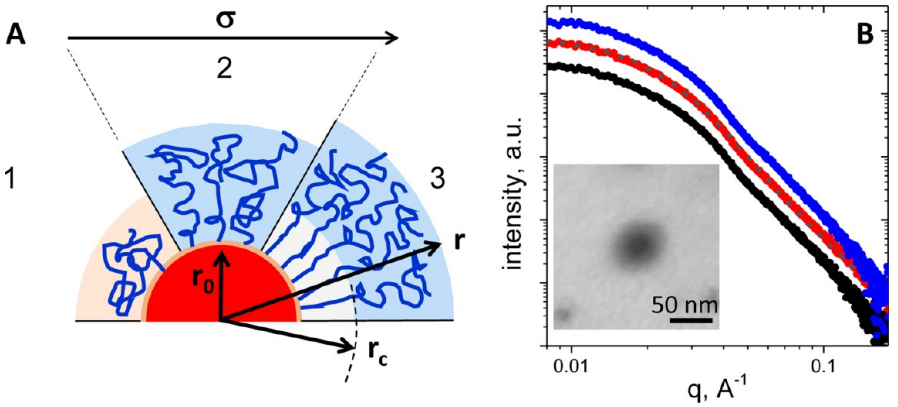

Figure 1. Isolated hairy nanoparticle (HNP) architecture: (A) Schematic of polymer brush morphology on nanoparticle and within a medium as a function of graft density depicting mushroom (1); semidiluted polymer bush (SDPB) (2); and concentrated polymer brush (CPB) regimes (3); where nanoparticle radius is r_0, HNP radius is r, and the transition radius between CPB and SDPB regions is r_c. (B) Small-angle X-ray patterns and form-factor model of THF solutions of 120 kDa polystyrene (PS)−silica (r_0 = 8 nm) HNPs (σ = 0.01 (black), 0.05 (red), 0.1 (blue) chains/nm^2). Dashed line through SiPS0p05 data is sphere form factor for a dilute solution of particles with r = 8 nm and log-normal distribution breadth β = 0.35. The data, which otherwise overlap perfectly, have been shifted for clarity. Dilution of the solution uniformly decreases the intensity, indicating the particles are dilute and not interfering. No agglomeration is observed in the data at low q, which is consistent with dynamic light scattering data obtained from the THF solutions. Inset: low voltage transmission electron microscopy image of a single HNP with a visible silica core and PS corona.

is the chain contour length. The transition between CPB and SDPB was worked out by Daoud and Cotton[16] and extended for systems with an inorganic core by Ohno et al.[9] and depends on r_o^{-1}, σ, N, and solvent (Table 1, Figure 1). Such a description provides a framework to discuss and understand the radial profile of local monomer density and the penetrability of the corona by the surrounding solvent medium. This surrounding medium may be a small molecule solvent, a linear polymer chain, or the swellable corona of an adjacent HNP. For example, for intermediate and high graft densities where the majority of the corona is in the CPB region, only minor interpenetration between adjacent coronas is anticipated. This is consistent with recent reports by Bockstaller[10,19] and Kumar[20] that the nanoparticle dynamics in this regime can be described as isolated particles suspended in a matrix.

Herein, we report the correlation between the order within hairy nanoparticle assemblies (aHNPs) and the solution architecture of the polymeric corona (CPB-to-SDPB regime) at low to intermediate graft densities where substantial penetration between adjacent coronas. This corresponds to HNPs with polymer grafts well above the entanglement molecular weight. Here the aHNP morphology evolves under viscoelastic deformation analogous to semicrystalline polymers, including the ability to undergo shape memory programming. This implies substantial interpenetration and chain entanglement between coronas of adjacent HNPs. Finally, noncubic local order, such as particle strings, is observed when the CPB−SDPB transition is approximately the particle radius and likely reflects an interplay between brush−brush wettability, depletion, and incompressibility factors that arise within the geometric confinement of the packed HNPs.

RAFT polymerization of polystyrene (PS) from 16 nm silica particles (Nissan) results in clear THF solutions (4 wt %) of HNPs with 120 kDa PS grafts at low to intermediate density[18] (Figure 1) (see Supporting Information for Experimental Details − SI-A). Small-angle X-ray scattering of dilute solutions (2 vol %) confirms core size and absence of aggregation (Figure 1B). Low-voltage transmission electron microscopy (TEM) of solutions dried onto TEM grids reveals spherical, irregular silica cores with a relatively broad size distribution that are surrounded by a thin organic shell (inset Figure 1B).

Following the models of Ohno and WZ,[9,17] the corona architecture of a nanoparticle of r_0 = 8 nm with grafts of N = 1150 ($M_w \sim$ 120 kDa, $R_{g,theta} \sim$ 9.8 nm[21]) will be fully in the SDPB regime for $\sigma < 0.025$ chains/nm^2 and fully in the CPB regime for $\sigma > 1$ chains/nm^2 (Figure 1A−3). At graft densities between these bounds, the portion of the corona in the CPB regime, r_c, will radially increase from the NP surface with increasing graft density. Note that for $\sigma < \sigma_c \sim 1/R_g^2$ (~0.01 chains/nm^2) there are insufficient chains to surround the particle, and the corona is sparse and in the mushroom regime. As such, PS graft densities with $\sigma \sim \sigma_c$, $r_0 \sim r_c$, and $r_0 < r_c$ (0.01, 0.05, and 0.1 chains/nm^2, respectively) will be discussed to understand the impact of corona architecture and its potential swellability by adjacent coronas on the structure, corona entanglement, and viscoelastic elongational characteristics of aHNPs (Table 1).

Removal of THF produces matrix-free aHNP films that are clear and transparent (Figure 2A). TEM images of the films

dx.doi.org/10.1021/mz4001805 | ACS Macro Lett. 2013, 2, 670−676

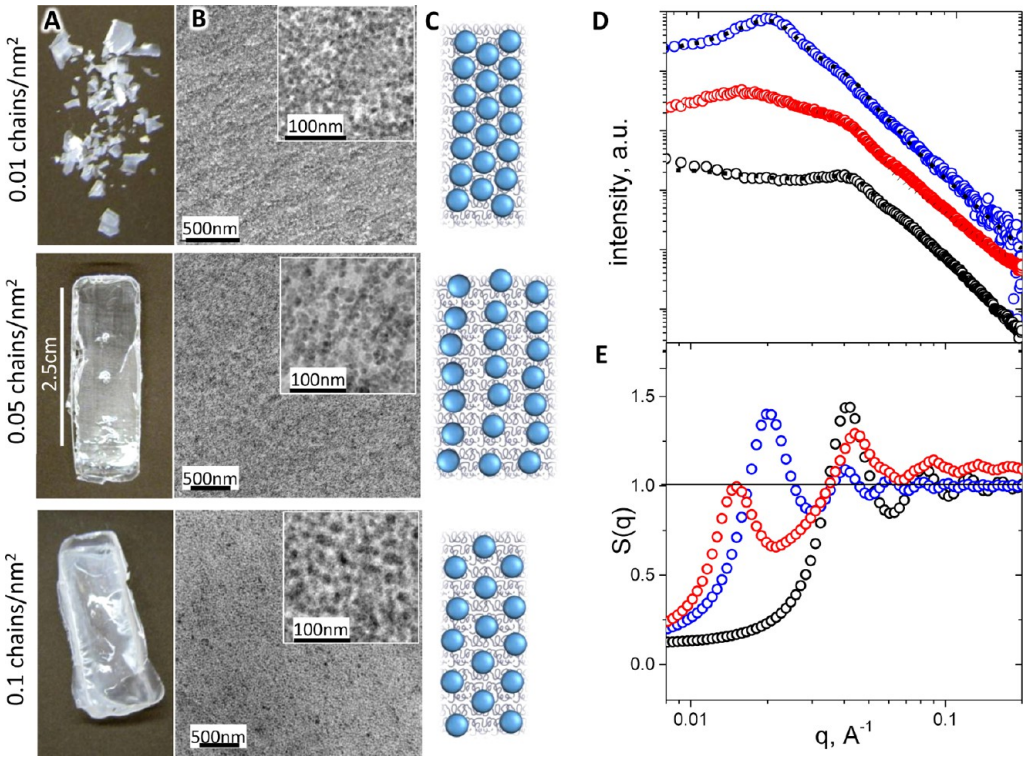

Figure 2. Assemblies of HNPs (aHNPs): (A) Macroscopic films of aHNPs after drying from THF. (B) Transmission electron micrographs of films from SiPS0p01, SiPS0p05, and SiPS0p1 (Table 1, and SI-B, Supporting Information, for larger images). (C) Schematic of local nanoparticle arrangement in the aHNP. (D) Small-angle X-ray patterns and (E) experimental structure factor of dried films, aged 1 year (black ○ SiPS0p01, red ○ SiPS0p05, blue ○ SiPS0p1). Lines in D are model scattering curves using the experimental solution form factor and the structure factor from data fit with a Percus and Yevick[32] hard sphere model (see SI-A, Supporting Information, for details). The scattering intensity for SiPS0p01 and SiPS0p1 agrees well with a single isotropic structure factor and the solution form factor (dashed lines). Two interference peaks for SiPS0p05 can be partially described by two independent structure factors (dotted line); however, intermediate and high q deviations from such a model indicate coupled interference, implying a single, locally nonisotropic HNP arrangement.

reveal densely packed SiO_2 nanoparticles (Figure 2B) with relatively short-range order. As with mesophase formation of block copolymers,[22] the extent of long-range structural order will depend on the geometrical dispersity of the building block, such as for HNP, the corona, and the core. Note that prior reports of single monolayer assemblies of HNPs with the same polydisperse silica core revealed long-range hexagonal close-packed structures,[8,10] implying that the relative softness of the corona and dispersity in grafts may partially compensate the effects of a broad distribution of core size. At the lowest PS graft density (0.01 chains/nm^2), the films are brittle at room temperature and very difficult to remove from the mold without fracturing. For these films (SiPS0p01), the nearest-neighbor spacing, L_{SAX}, is 18 nm as revealed by the first structure factor peak from small-angle X-ray scattering (SAX) (Figure 2D, Table 1). The total SAX scattering curve is also well described by a single population of particles with hard-sphere interference and short-range order (particle form factor (Figure 1B) and a single hard sphere structure factor).[8] Furthermore, the average particle spacing is consistent with a densely packed geometrical model of silica particles surrounded by dense polystyrene, where the volume fraction of inorganic is determined from TGA (L_{TGA} = 19 nm, Table 1, Figure 2D). The highest graft density (SiPS0p1, σ = 0.1 chains/nm^2) exhibits a similar SAXS pattern with an interference at L_{SAX} = 31 nm (Figure 2D, Table 1). This is also consistent with the experimental silica fraction and model (L_{TGA} = 32 nm) with short-range order. The few literature reports of aHNPs discuss systems with σ > 0.2 chains/nm^2 and brushes mostly in the CPB regime.[8,19,23] These systems also exhibit isotropic particle arrangement ranging from disordered with short-range order (as with SiPS0p1) to close-packed arrangements and follow trends seen for star colloids.[24,25]

In contrast to the aHNPs with high and low graft densities, two incommensurate SAX peaks (42 nm, 17 nm, Figure 2D) are observed when $r_0 \sim r_c$, and the entire PS corona is in the SDPB region (SiPS0p05). These values are not consistent with order reflections of lamella or closed-packed arrangements, nor do they describe a simple disordered assembly of hard spheres with short-range order. Also, a hard sphere model with short-range order anticipates a center−center distance of silica cores of 26 nm. Alternatively, the SAX pattern could be accounted for by a phase-separated morphology consisting of two regions of particles with different separation. Following this hypothesis, the interference peaks can only be partially described by the particle form factor and two independent hard sphere structure factors; however, intermediate and high q deviations from such a model indicate coupled interference, which is consistent with a single, locally nonisotropic HNP arrangement (Figure 2D). Furthermore, no indication of phase-separated regions can be found in the low voltage TEM or in an increased scattering at low q that would reflect density differences between the domains. Rather, TEM images under high magnification reveal particle string formation (Figure 2B) that is verified by digital Fourier transform of the TEM image (see SI-B, Supporting Information). Note that the samples are >10 000 times thicker

dx.doi.org/10.1021/mz4001805 | ACS Macro Lett. 2013, 2, 670−676

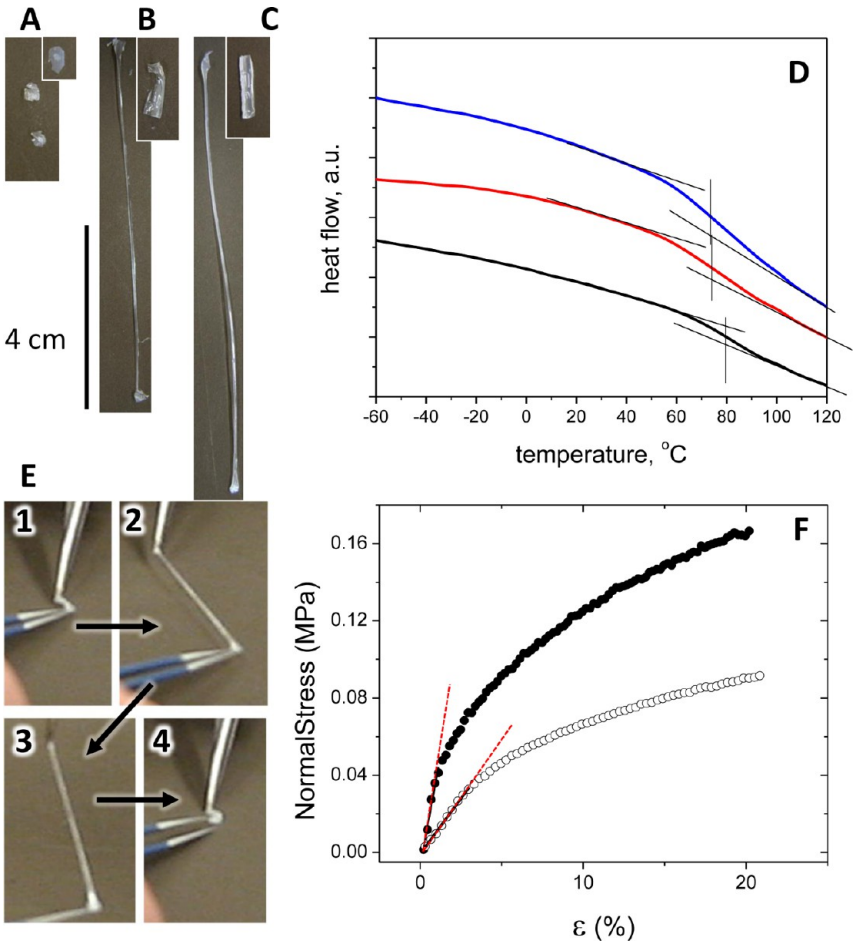

Figure 3. Thermomechanical properties of aHNPs: as-cast aHNP films before and after elongation. (A) SiPS0p01, (B) SiPS0p05, and (C) SiPS0p1. (D) Differential scanning calorimetry (second heating) for SiPS0p01 (black), SiPS0p05 (red), and SiPS0p1 (blue). (E) Shape memory process (5th cycle) of SiPS0p05. 1: Short piece of sample at room temperature is heated over the hot plate and 2: stretched at ∼100 °C. 3: The deformation is temporarily fixed by quenching to RT and 4: recovered by reheating to ∼100 °C over the hot plate. (F) Stress−strain curve from dynamic mechanical analysis for SiPS0p1 (filled circles) and neat PS (open circles) at T = 110 °C. Dashed lines in F are linear fits to data to obtain Young's modulus: $E_{SiPS0p1}$ = 0.05 MPa, E_{PS} = 0.012 MPa.

than an individual HNP. Thus, surface-induced ordering effects[26] are not relevant, nor are they observed at the bulk interfaces (see SI-B, Figure S1E, F, Supporting Information).

The nonisotropic local order in SiPS0p05 may be understood from one of two perspectives: solution-assembled, kinetically trapped structures or as a free energy minimum arrangement of the aHNP. Numerous experimental and theoretical studies of nanoparticle assembly have demonstrated symmetry breaking for sequential nanoparticle assembly, where an assembled NP dimer in solution displays an orientationally dependent interaction with a subsequent isotropic NP monomer.[27−29] In the solvent-free bulk state, packing constraints and very long relaxation times for the extremely large HNP could effectively hinder these string-like structures from adopting an isotropic local packing. Alternatively, a manifold of free energy minima may exist that optimizes the relative conformational freedom of the end-tethered chains within the intervening volume occupied by end-tethered chains attached to adjacent NPs. In other words, the characteristics of the corona (graft density and chain molecular weight) will determine not only the extent of interpenetrability between coronas (i.e., dry or wet brush) but also the distribution of penetrability around the HNP in the highly nonuniform intervening space of the solvent-free, close packed nearest neighbors. For example since the volume per chain increases with distance from the nanoparticle surface, a nonuniform spherical distribution of chain volume that includes a small fraction of highly confined regions at the equator (i.e., sheets) or poles (i.e., string) compensated by a greater volume between particles in an orthogonal direction may increase the total conformation entropy relative to a uniform polymer shell. For chains on a single particle, some must be stretched more than others to uniformly occupy the effective interstitial sites whether the assembly is disordered or ordered. Additional theory and experiments are definitely necessary to clarify the predominant kinetic and thermodynamic factors, but some experimental observations of agglomerates in matrix-rich, HNP−polymer systems support the observation of non-isotropic arrangement in aHNPs. Kumar et al. reported a region within the PS−silica HNP−PS matrix system where connected sheets and string agglomerates form.[7,30,31] When the molecular weight of the graft and matrix are comparable, these novel aggregates occur in a narrow graft density region ($0.05 \leq \sigma \leq 0.1$ chains/nm^2) that is bracketed by spherical aggregates and dispersed silica. The strings and sheets structures are speculated to form at the boundary of macroscale aggregation and dispersion due to a balance in matrix penetrability of the corona and chain depletion effects. Conceptually, similar physics could underlie the structures when adjacent coronas

dx.doi.org/10.1021/mz4001805 | ACS Macro Lett. 2013, 2, 670−676

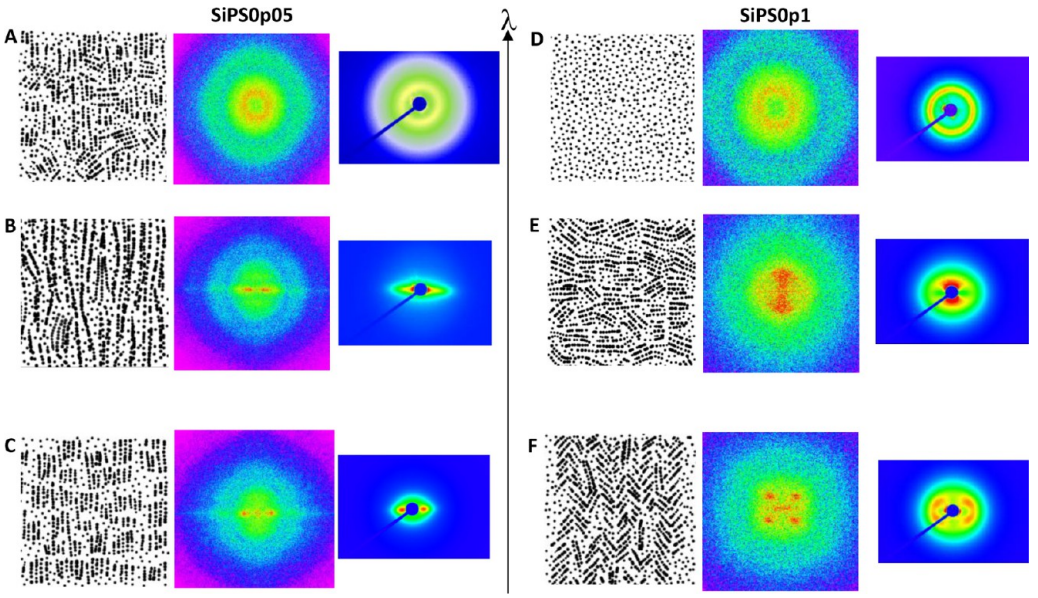

Figure 4. aHNP morphology evolution during deformation. Deformation direction is vertical (arrow, λ). Left: SiPS0p05. Right: SiPS0p1. Three columns are presented for each sample. Column 1 contains a schematic representation of possible morphology; column 2 contains a digital Fourier transform of the schematic in column 1; and column 3 contains the experimental 2D SAX pattern. Rows A (SiPS0p05) and D (SiPS0p1) show unstretched data; rows B and E show data for $\lambda = 3$; and rows C and F show data for $\lambda = 1.5$ (recovered). Note that deformed polystyrene of molecular weight comparable to the grafted chains does not exhibit similar features (see SI-C, Supporting Information).

penetrate in the aHNP and may explain the string formation in SiPS0p05 which is in the same graft density regime.

Figure 3 summarizes the thermomechanical characteristics of as-cast aHNPs films. DSC (Figure 3D) and DMA (not shown) reveal a thermally broad glass transition (T_g) and accompanying softening around ~80 °C. This relatively low T_g with respect to bulk PS (110 °C) has been observed in other PS-based aHNPs; for example, Tchoul et al. reported a PS−TiO_2 aHNP (100 kDa PS at $\sigma \sim 0.03$ nm^{-2}) with a comparable T_g, whereas the same system with chains untethered regained the T_g of the matrix polymer.[11] The broadness and reduced T_g likely reflect the frustrated packing and increased local free volume of the tethered polymer within the nanoscopic spaces between the nanoparticle cores ($L - 2r_0 \sim R_g$).

The qualitative deformability above T_g of the as-cast aHNP films is shown in Figure 3A−C. The sparse PS corona at $\sigma \sim \sigma_c$ (SiPS0p01) results in low tenacity and immediate beading of the material into droplets. This implies weak entanglement between NP coronas. In contrast, the thicker PS corona of SiPS0p05 and SiPS0p1 enables elongation to several times the original length. This implies relatively strong entanglement between adjacent HNP coronas. This behavior is qualitatively similar to neat 100 kDa polystyrene under a comparable elongation rate (aHNP $\lambda_{max} \sim 5$, PS $\lambda_{max} \sim 3$). However, both the modulus and stress level in the plastic regime at 110 °C for SiPS0p1 are twice that of neat PS (Figure 3F). This is consistent with prior reports of mechanical property enhancement of conventional nanocomposite elastomers with spherical nanoparticle inclusions at comparable inorganic loadings (~10 vol %).[33,34] Interestingly, at deformation rates of 0.25 cm/s, the majority of the mechanical energy can be stored in the aHNP by rapidly quenching through T_g. The result is that SiPS0p1 and SiPS0p05 exhibit reasonable shape memory behavior (Figure 3E, recovery ratio 95%, SI-F, Supporting Information). In contrast un-cross-linked PS dissipates mechanical energy at comparable deformation rates and thus does not exhibit as much shape recovery (recovery ratio 85%). The extent of mechanical energy storage in viscoelastic un-cross-linked systems is inversely proportional to the rate of chain relaxation (i.e., stress relaxation and creep) at the shape setting temperature ($T > T_g$). Thus, the difference in shape memory behavior emphasizes the substantially lower cooperative relaxation rates of the entangled chain decorating the NP relative to the entangled untethered chain. This is even more impressive noting that for the same shape setting temperature (100 °C) the deformation of aHNP was carried out at temperatures deeper in the melt region than PS (PS $T/T_g \sim 1$, aHNP $T/T_g \sim 0.8$).

Although SiPS0p05 and SiPS0p1 behave mechanically similar, their morphology development during uniaxial elongation is very different (Figure 4). The initial films are homogeneous, consisting of a random distribution of the locally structured domains as revealed by the uniform azimuthal intensity distribution in two-dimensional SAX (Figure 4A, D). Upon stretching SiPS0p05 to $\lambda = 3$, a featureless equatorial streak develops (Figure 4B). This implies that while mesoscopic features align the interparticle distance of the initial string-like assemblies is disrupted, and coherence is lost. The general mesoscale alignment is reminiscent of polymer nanocomposites containing anisotropic fillers (e.g., carbon nanotubes[35] or magnetically aligned silica nanoparticles[36]) where the extended structures rotate *parallel* to the deformation direction. Upon recovery, the 2D SAX pattern exhibits a two-point pattern (Figure 4C), indicating the reorganization of the laterally uncoordinated strings into domains with coherence similar to the initial state (42 nm), however, now preferentially aligned along the deformation direction. In contrast, SiPS0p1 forms a broad diffuse lobe on the meridian when stretched to $\lambda = 3$ (Figure 4E), reflecting the alignment of larger scatterers *orthogonal* to the elongation direction. A possible real-space morphology that agrees with SAX consists of domains that are aligned perpendicular to the deformation direction that

dx.doi.org/10.1021/mz4001805 | *ACS Macro Lett.* 2013, 2, 670−676

resembles rafts of nanoparticles formed in stretched filled elastomers due to affine deformation.[37] Upon recovery, SiPS0p1 shows the formation of a four-point pattern, indicating the uniaxial contraction of scattering features from the deformed sample into a chevron-type morphology (Figure 4F). Overall this morphology evolution is similar to observations made for thermoplastic polymers in which crystalline domains form tilted arrangements depending on the extent of deformation.[38] Schematics, and associated digital Fourier transform (DFT), of the proposed morphology evolution of SiPS0p05 and SiPS0p1 are compared in Figure 4 with the experimental scattering patterns (see SI-D, Supporting Information).

The stark difference in the morphological evolution of these two aHNPs upon deformation must reflect a difference in strain distribution in the initial local NP arrangement. Viscoelastic deformation occurs in the PS-rich regions. For SiPS0p05, the nonisotropic NP arrangement likely results in a nonuniform local strain distribution producing shear that aligns the domains along the deformation direction. Concurrently, the interpenetrability of the corona with adjacent coronas may be nonuniform, reflecting the two different particle−particle spacings. Therefore, local deformation will occur along the weakest direction. On the other hand, SiPS0p1 is locally isotropic. The formation of domains perpendicular to the deformation agrees with results from a conventional nanocomposite system involving silica particles[37] and must be a result of extension of entangled corona chains parallel to the deformation direction. Affine deformation implies a lateral compression which drives the system into a layered morphology.

In conclusion, it is shown that the structure and viscoelastic elongational characteristics of aHNPs depend on architectural details of the polymeric corona of the individual HNP. Nanoparticles with highly penetrable coronas ($r_c \sim r_o$) assemble into locally anisotropic structures, a phenomenon that has previously only been observed for HNPs in the presence of polymer matrices of varying molecular weight.[5,6] The anisotropy (habit) of the HNP-rich phase in prior studies of these blends could arise from processing, matrix effects, or underlying HNP−HNP interactions. Since neat aHNP is a bulk version of the aggregated phase in these binary blends, the results presented herein indicate that HNP−HNP interactions are crucial to this morphology control. As such, we suspect the underlying energetics and mechanism of aHNP structure formation are analogous to these blends, where conceptually matrix−brush penetrability is replaced by brush−brush penetrability.[13] Specifically, intermediate graft density (SiPS0p05) leads to the formation of strings which optimize configurational freedom of the tethered chains within the confining volume of the surrounding nanoparticles. Viscoelastic behavior implies these chains are entangled, and the coronas are mutually swollen. The NP arrangement within this aHNP responds to elongation similar to a rigid body and displays characteristics qualitatively similar to semiflexible rods dispersed in the amorphous polymer matrix.[35] Alternatively, a locally isotropic, mutually entangled HNP assembly deforms uniaxially in a manner similar to strain-induced crystallites in a semicrystalline polymer.[38] This implies a hierarchy of relaxation times between cooperative chain motion within the corona and collective motion within and of the local NP architecture. Overall these findings indicate intriguing parallels between aHNP and other mesoscale ordered polymeric systems including hard−soft block copolymers and semicrystalline polymers. To address the fundamental thermodynamic and kinetic factors, however, HNP systems with higher purity and lower dispersity of core, corona size, and architecture are required. In parallel, technological relevance requires a more detailed understanding of the relaxation and aging processes and their impact on physical properties. Nevertheless, with the appropriate corona architecture, aHNPs afford opportunities to design high inorganic fraction hybrids that retain processability to create thin films or fibers for next-generation dielectrics or gradient refraction index materials for optoelectronic applications.

■ ASSOCIATED CONTENT

Ⓢ Supporting Information

Experimental details on processing and characterization; TEM and digital Fourier transform; SAX of polystyrene under deformation; SAX profiles of aHNP under deformation; and video of shape memory process of aHNP. This material is available free of charge via the Internet at http://pubs.acs.org.

■ AUTHOR INFORMATION

Corresponding Author

*E-mail: richard.vaia@wpafb.af.mil.

Notes

The authors declare no competing financial interest.

■ ACKNOWLEDGMENTS

Funding provided by the Air Force Office of Scientific Research is gratefully acknowledged. The authors would like to thank Peter Mirau for NMR measurements, Pamela Lloyd for TEM (AFRL/RX), Marlene Houtz for DSC measurements (University of Dayton Research Institute), and Alexander Hexemer and Eric Schaible for assistance with experiments at the SAXS/WAXS beamline 7.3.3 of the Advanced Light Source at Lawrence Berkeley National Laboratory, supporting this research. The authors thankfully acknowledge Dr. Sanat Kumar (Columbia University), Dr. Linda Schadler, and Dr. Douglas Dukes (Rensselaer Polytechnic Institute) for helpful discussions regarding this work.

■ REFERENCES

(1) Winey, K. I.; Vaia, R. A. *MRS Bull.* **2007**, *32*, 314−322.
(2) Vaia, R. A. *Abstr. Pap. - Am. Chem. Soc.*, 221st IEC, 2001; p 290.
(3) Kumar, S. K.; Krishnamoorti, R. *Ann. Rev. Chem. Biomol. Eng.* **2010**, *1*, 37−58.
(4) Vaia, R. A.; Maguire, J. F. *Chem. Mater.* **2007**, *19*, 2736−2751.
(5) Akcora, P.; Liu, H.; Kumar, S. K.; Moll, J.; Li, Y.; Benicewicz, B. C.; Schadler, L. S.; Acehan, D.; Panagiotopoulos, A. Z.; Pryamitsyn, V.; Ganesan, V.; Ilavsky, J.; Thiyagarajan, P.; Colby, R. H.; Douglas, J. F. *Nat. Mater.* **2009**, *8*, 354−359.
(6) Coppee, S.; Gabriele, S.; Jonas, A. M.; Jestin, J.; Damman, P. *Soft Matter* **2011**, *7*, 9951.
(7) Moll, J.; Akcora, P.; Rungta, A.; Gong, S.; Colby, R. H.; Benicewicz, B. C.; Kumar, S. K. *Macromolecules* **2011**, *44*, 7473−7477.
(8) Goel, V.; Pietrasik, J.; Dong, H.; Sharma, J.; Matyjaszewski, K.; Krishnamoorti, R. *Macromolecules* **2011**, *44*, 8129−8135.
(9) Ohno, K.; Morinaga, T.; Takeno, S.; Tsujii, Y.; Fukuda, T. *Macromolecules* **2007**, *40*, 9143−9150.
(10) Choi, J.; Hui, C. M.; Pietrasik, J.; Dong, H.; Matyjaszewski, K.; Bockstaller, M. R. *Soft Matter* **2012**, *8*, 4072.
(11) Tchoul, M. N.; Fillery, S. P.; Koerner, H.; Drummy, L. F.; Oyerokun, F. T.; Mirau, P. a.; Durstock, M. F.; Vaia, R. a. *Chem. Mater.* **2010**, *22*, 1749−1759.

(12) Tang, C.; Bombalski, L.; Kruk, M.; Jaroniec, M.; Matyjaszewski, K.; Kowalewski, T. *Adv. Mater.* **2008**, *20*, 1516−1522.
(13) Fernandes, N. J.; Koerner, H.; Giannelis, E. P.; Vaia, R. A. *MRS Commun.* **2013**, *3* (01), 13−29.
(14) Alexander, S. *J. Phys. (Paris)* **1977**, *38*, 983−987.
(15) de Gennes, P. G. *Macromolecules* **1980**, *13*, 1069−1075.
(16) Daoud, M.; Cotton, J. *J. Phys. (Paris)* **1982**, *43*, 531−538.
(17) Wijmans, C. M.; Zhulina, E. B. *Macromolecules* **1993**, *26*, 7214−7224.
(18) Li, C.; Benicewicz, B. C. *Macromolecules* **2005**, *38* (14), 5929−5936.
(19) Choi, J.; Hui, C. M.; Schmitt, M.; Pietrasik, J.; Margel, S.; Matyjazsewski, K.; Bockstaller, M. R. *Langmuir* **2013**, *29* (21), 6452−6459.
(20) Dukes, D.; Li, Y.; Lewis, S.; Benicewicz, B. C.; Schadler, L.; Kumar, S. K. *Macromolecules* **2010**, *43*, 1564−1570.
(21) Ken, T.; Farmer, B. S.; Nakamura, Y.; Iatrou, H.; Hong, K.; Mays, J. W. *Macromolecules* **2005**, *38*, 1447−1450.
(22) Segalman, R. A.; Hexemer, A.; Hayward, R. C.; Kramer, E. J. *Macromolecules* **2003**, *36*, 3272−3288.
(23) Matyjaszewski, K.; Tsarevsky, N. V. *Nat. Chem.* **2009**, *1*, 276−288.
(24) Watzlawek, M.; Likos, C. N.; Loewen, H. *Phys. Rev. Lett.* **1999**, *82*, 5289−5292.
(25) Likos, C. N. *Phys. Rep.* **2001**, *348*, 267−439.
(26) Voudouris, P.; Choi, J.; Gomopoulos, N.; Sainidou, R.; Dong, H.; Matyjaszewski, K.; Bockstaller, M. R.; Fytas, G. *ACS Nano* **2011**, *5* (7), 5746−5754.
(27) Nepal, D.; Park, K.; Vaia, R. A. *Small* **2012**, *8*, 1013.
(28) Liu, K.; Nie, Z.; Zhao, N.; Li, W.; Rubinstein, M.; Kumacheva, E. *Science* **2010**, *329*, 197.
(29) Yang, M.; Chen, G.; Zhao, Y.; Silber, G.; Wang, Y.; Xing, S.; Han, Y.; Chen, H. *Phys. Chem. Chem. Phys.* **2011**, *12*, 11850.
(30) Maillard, D.; Kumar, S. K.; Fragneaud, B.; Kysar, J., A.; Rungta, A.; Benicewicz, B. C.; Deng, H.; Brinson, L. C.; Douglas, J. F. *Nano Lett.* **2012**, *12*, 3909−3914.
(31) Akcora, P.; Kumar, S. K.; Garcia Sakai, V.; Li, Y.; Benicewicz, B. C.; Schadler, L. S. *Macromolecules* **2010**, *43*, 8275−8281.
(32) Percus, J. K.; Yevick, G. J. *J. Phys. Rev.* **1958**, *110*, 1.
(33) Crosby, A. J.; Lee, J. Y. *Polym. Rev.* **2007**, *47*, 217−229.
(34) Bergstrom, J. S.; Boyce, M. C. *Rubber Chem. Technol.* **1999**, *72*, 633−656.
(35) Koerner, H.; Liu, W.; Alexander, M.; Mirau, P.; Dowty, H.; Vaia, R. A. *Polymer* **2005**, *46* (12), 4405−4420.
(36) Robbes, A.-s.; Cousin, F.; Meneau, F.; Dalmas, F.; Jestin, J.; Saclay, C. E. A.; Cedex, G.-s.-y. *Macromolecules* **2011**, *44*, 8858−8865.
(37) Rharbi, Y.; Cabane, B.; Vacher, A.; Joanicot, M.; Boue, F. *Europhys. Lett.* **1999**, *46* (4), 472.
(38) Koerner, H.; Kelley, J. J.; Vaia, R. A. *Macromolecules* **2008**, *41* (13), 4709−4716.